Interaction of a Peptide from the Pre-transmembrane Domain of the Severe Acute Respiratory Syndrome Coronavirus Spike Protein with Phospholipid Membranes

Jaime Guillén, Miguel R. Moreno, Ana J. Pérez-Berná, Angela Bernabeu, and José Villalaín*

Instituto de Biología Molecular y Celular, Campus de Elche, Universidad "Miguel Hernández", E-03202 Elche-Alicante, Spain

Received: May 14, 2007; In Final Form: September 25, 2007

The severe acute respiratory syndrome coronavirus (SARS-CoV) envelope spike (S) glycoprotein, a Class I viral fusion protein, is responsible for the fusion between the membranes of the virus and the target cell. In order to gain new insight into the protein membrane alteration leading to the viral fusion mechanism, a peptide pertaining to the putative pre-transmembrane domain (PTM) of the S glycoprotein has been studied by infrared and fluorescence spectroscopies regarding its structure, its ability to induce membrane leakage, aggregation, and fusion, as well as its affinity toward specific phospholipids. We demonstrate that the SARS-CoV PTM peptide binds to and interacts with phospholipid model membranes, and, at the same time, it adopts different conformations when bound to membranes of different compositions. As it has been already suggested for other viral fusion proteins such as HIV gp41, the region of the SARS-CoV protein where the PTM peptide resides could be involved in the merging of the viral and target cell membranes working synergistically with other membrane-active regions of the SARS-CoV S glycoprotein to heighten the fusion process and therefore might be essential for the assistance and enhancement of the viral and cell fusion process.

Introduction

A new infectious disease, defined as severe acute respiratory syndrome or SARS, emerged in Southern China in the autumn of 2002 and was originated by a novel type of coronavirus, SARS-CoV. This disease, which infects humans causing an atypical and often lethal pneumonia, spread to more than 20 countries in Asia, North America, South America, and Europe in the spring of 2003.[1−5] Approximately 8400 people worldwide suffered from SARS, and more than 800 deaths were recognized according to the World Health Organization. It was hypothesized that the new virus was originated from wild animals, and promptly a coronavirus was identified in civet cats from Southern China with a sequence identity of more than 99% to the SARS-CoV. Therefore, the possibility of a future outbreak coming out from a natural reservoir cannot be ruled out.

Coronaviruses are a diverse group of enveloped, positive-stranded RNA viruses, with 3−4 proteins embedded in the envelope, that cause respiratory and enteric diseases in humans and other animals. SARS-CoV infection, similarly to other envelope viruses, is achieved through fusion of the lipid bilayer of the viral envelope with the host cell membrane. The SARS-CoV virion, as with other coronaviruses, consists of a nucleocapsid core surrounded by a envelope containing three membrane proteins: spike, membrane, and envelope proteins. The spike glycoprotein S, responsible for the characteristic spikes of the SARS-CoV, is a surface glycoprotein that mediates viral entry by binding to the cellular receptor angiotensin-converting enzyme 2[6] and induces membrane fusion. In some strains, protein S is cleaved by a protease to yield two noncovalently associated subunits, S1 and S2 (Figure 1), but cleavage is not an absolute requirement for the mechanism of fusion.[7] The receptor binding domain, localized in domain S1 and mapped to amino acids 318−510,[8,9] defines the host range of the virus,[10] while S2 is responsible for the fusion between the viral and cellular membranes.[10,11] S2 contains two highly conserved heptad repeat regions (HR1 and HR2),[12−18] similarly to other viral fusion proteins, including HIV-1 gp41, influenza hemagglutinin HA2, Ebola virus glycoprotein, and paramyxovirus F protein.[19−22] All of them have been classified as Class I transmembrane glycoproteins and are displayed on the surface of the viral membrane as oligomers. Class I viral proteins also contain a hydrophobic region denoted as the fusion peptide (FP) and another hydrophobic region immediately adjacent to the membrane-spanning domain denoted as the pre-transmembrane domain (PTM). Under the current model for membrane fusion, there are at least three conformational states of the envelope fusion protein: the pre-fusion native state, the pre-hairpin intermediate state, and the post-fusion hairpin state.[23−27] The first step in membrane fusion involves the exposure of the FP and, later on, its insertion into the host cell lipid bilayer. Subsequently, the heptad repeat regions HR1 and HR2 are exposed in an intermediate state binding each other to form a coiled-coil structure facilitating the juxtaposition of the FP and PTM segments, bringing in close proximity the viral and cellular membranes; this is followed by virus-cell membrane fusion and viral entry.

Studies with a number of viral fusion proteins have shown that the region immediately adjacent to the membrane-spanning domain plays an essential role in the fusogenic activities of these proteins, being a common characteristic to other Class I viral fusion proteins of several virus families.[28−33] For example, the membrane-proximal domain of HIV-1 gp41 contains several Trp residues that are invariant between different strains, and deletion of this membrane-proximal region or substitution of the conserved Trp residues blocked the cell−cell fusion activity of gp41.[30] Through experiments using synthetic peptides

* Corresponding author. Address: Instituto de Biología Molecular y Celular, Universidad "Miguel Hernández", E-03202 Elche-Alicante, Spain. Tel: +34 966 658 762. Fax: +34 966 658 758. E-mail: jvillalain@umh.es.

10.1021/jp073675y CCC: $37.00
Published on Web 11/17/2007

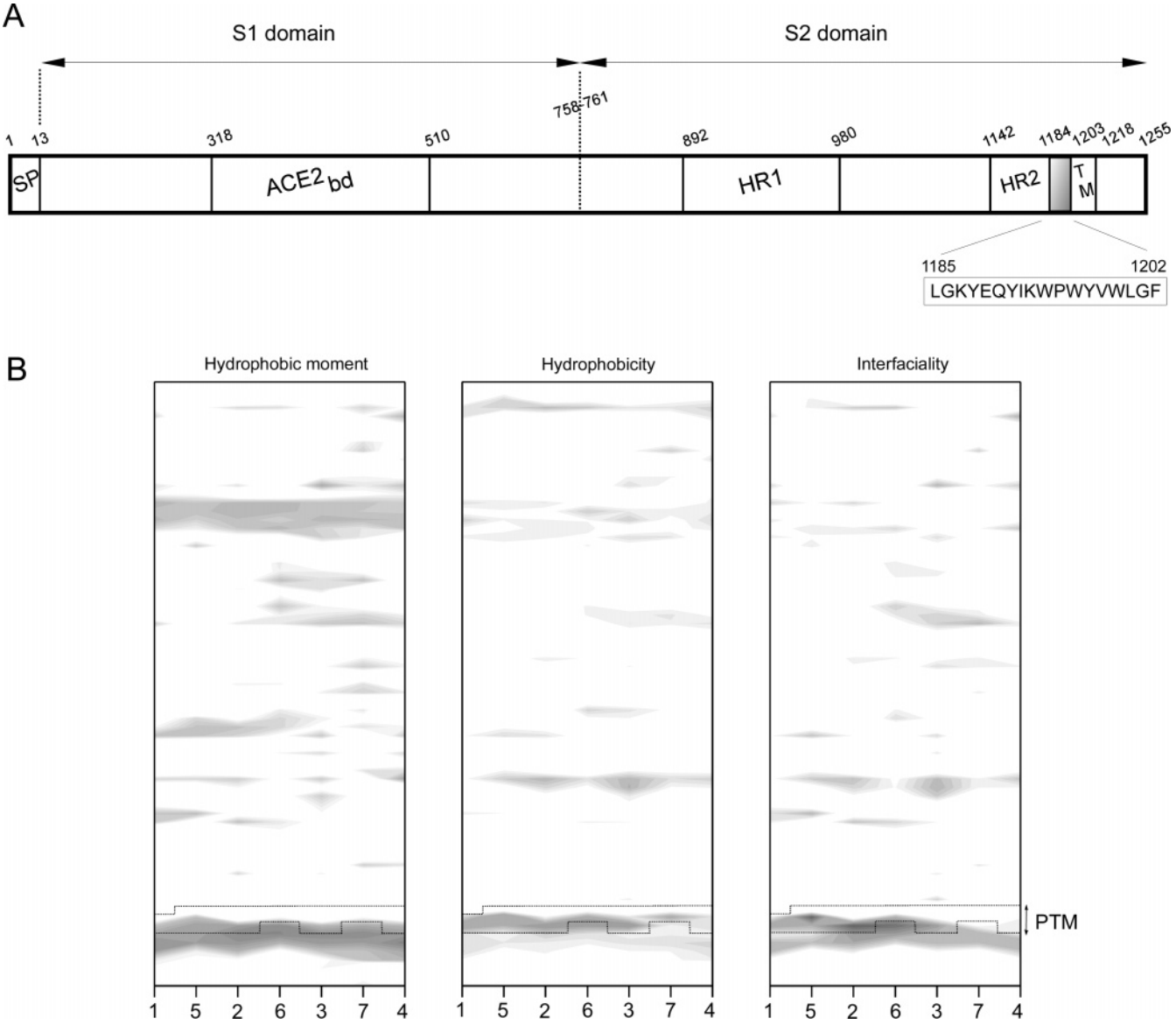

Figure 1. (A) Schematic view of the organization of SARS-CoV spike glycoprotein S (amino acid residues 1−1255 for the full length), as well as the S1 and S2 subunits, showing the approximate structural and functional regions: the N-terminal signal peptide (SP), the ACE2 binding domain, the transmembrane domain (TM), and the predicted heptad repeat regions pertaining to the S2 subunit, HR1 and HR2. The fusion domain is located at the N-terminus of the S2 subunit. Also shown is the sequence of the peptide used in this work. It should be noted that the size of each domain is not drawn to an exact scale. (B) Hydrophobic moment, hydrophobicity, interfaciality distribution, and relative position of the peptide used in this study along the SARS-CoV spike S2 domain, assuming it forms an α-helical wheel (see ref 29 for details). Only positive bilayer-to-water transfer free-energy values are depicted (shaded areas).

analogous to the aromatic domains of HIV-1 and EboV, it has been demonstrated that these peptides may aid in the disruption of the viral membrane during fusion and are capable of inducing membrane leakage and lipid mixing of model phospholipid membranes.[28,29,34−38] Recently, the presence of this highly hydrophobic aromatic domain has been shown in SARS-CoV;[39,40] in addition, this region displays a surface patch with high bilayer-to-water transfer free-energy values (Figure 1). Interestingly, the PTM domain of coronavirus fusion proteins is highly conserved, having a high content of aromatic residues.

Although much information has been obtained in recent years on membrane fusion, we do not know yet the processes and the mechanism behind virus−host cell membrane fusion. Elucidating the nature of the interactions between phospholipids, membrane proteins, and peptides is essential for the understanding of the structure and function of membrane proteins, clarifying the specific roles of specific types of phospholipids in biological membranes. In the present work, we report our results on the determination of the secondary structure and the interaction with model membranes of a peptide pertaining to the aromatic pre-transmembrane domain of SARS-CoV (SARS-CoV PTM), the structural changes of which take place in both the peptide and phospholipid molecules, induced by membrane binding and interaction with the lipid bilayer through a series of complementary experiments such as leakage, fusion, and aggregation. Moreover, we show that SARS-CoV PTM strongly partitions into phospholipids membranes and can be localized at different depths depending on the phospholipid composition of the vesicles. These results would suggest that the SARS-CoV PTM could be involved in the merging of the viral and target cell membranes working synergistically with other membrane-active regions of the S spike glycoprotein.

Materials and Methods

Materials and Reagents. The synthetic peptide encompassing residues 1185−1202 of SARS-CoV ([1185]LGKYEQYIKW-

PWYVWLGF[1202]) was synthesized with N-terminal acetylation and C-terminal amidation on an automatic multiple synthesizer (Genemed Synthesis, San Francisco, CA). The peptide was purified by reverse-phase high-performance liquid chromatography to >95% purity, and its composition and molecular mass were confirmed by amino acid analysis and mass spectroscopy. Since trifluoroacetate has a strong infrared absorbance at approximately 1673 cm^{-1}, which interferes with the characterization of the peptide Amide I band,[41] residual trifluoroacetic acid, used both in peptide synthesis and in the high-performance liquid chromatography mobile phase, was removed by several lyophilization/solubilization cycles in 10 mM HCl.[42] Egg L-α-phosphatidylcholine (EPC), egg sphingomyelin (SM), bovine brain phosphatidylserine (BPS), egg trans-esterified L-α-phosphatidylethanolamine (TPE), bovine liver L-α-phosphatidylinositol (BPI), 1,2-dimyristoylphosphatidylcholine (DMPC), 1,2-dimyristoylphosphatidylglycerol (DMPG), 1,2-dimyristoylphosphatidylserine (DMPS), 1,2-dimyristoylphosphatidic acid (DMPA), 1-palmitoyl-2-oleoyl-phosphoethanolamine (POPE), cholesterol (Chol), lissamine rhodamine B 1,2-dihexadecanoyl-*sn*-glycero-3-phosphoethanolamine (*N*-Rh-PE), and *N*-(7-nitrobenz-2-oxa-1,3-diazol-4-yl)-1,2-dihexadecanoyl-*sn*-glycero-3-phosphoethanolamine (NBD-PE) were obtained from Avanti Polar Lipids (Alabaster, AL). 5-Carboxyfluorescein (CF, >95% by HPLC), 5-doxyl-stearic acid (5NS), 16-doxyl-stearic acid (16NS), sodium dithionite, deuterium oxide (99.9% by atom), Triton X-100, EDTA, and HEPES were purchased from Sigma-Aldrich (Madrid, Spain). 1,6-Diphenyl-1,3,5-hexatriene (DPH), and 1-(4-trimethylammoniumphenyl)-6-phenyl-1,3,5-hexatriene (TMA-DPH) were obtained from Molecular Probes (Eugene, OR). Porcine lungs were obtained from a local slaughterhouse. Plasma membrane (LE) from lung tissue pneumocytes was obtained according to ref 43, and lipid extraction was performed according to the Bligh and Dyer procedure using a ratio of 1:1:0.9 (v/v/v) between chloroform, methanol, and the corresponding aqueous sample.[44] All other chemicals were commercial samples of the highest purity available (Sigma-Aldrich, Madrid, Spain). Water was deionized, twice-distilled, and passed through Milli-Q equipment (Millipore Ibérica, Madrid) to a resistivity higher than 18 MΩ cm.

Sample Preparation. For FTIR spectroscopy, aliquots containing the appropriate amount of lipid in chloroform/methanol (2:1, v/v) were placed in a test tube containing 200 μg of dried lyophilized peptide. After vortexing, the solvents were removed by evaporation under a stream of O_2-free nitrogen, and, finally, traces of solvents were eliminated under vacuum in the dark for more than 3 h. The samples were hydrated in 200 μL of D_2O buffer containing 20 mM HEPES, 50 mM NaCl, and 0.1 mM EDTA, pH 7.4, and incubated at 10 °C above the phase transition temperature (T_m) of the phospholipid mixture with intermittent vortexing for 45 min to hydrate the samples and obtain multilamellar vesicles (MLVs). The samples were frozen and thawed five times to ensure complete homogenization and maximization of peptide/lipid contacts with occasional vortexing. Finally, the suspensions were centrifuged at 15 000 rpm at 25 °C for 15 min to remove the possible peptide unbound to the membranes. The pellet was resuspended in 25 μL of D_2O buffer and incubated for 45 min at 10 °C above the T_m of the lipid mixture, unless stated otherwise. Large unilamellar vesicles (LUVs) with a mean diameter of 100 nm (leakage assay) and 200 nm (fusion assays) were used to study vesicle leakage. They were prepared from MLVs in the absence of peptide by the extrusion method[45] using polycarbonate filters with a pore size of 0.1 and 0.2 μm (Nuclepore Corp., Cambridge, CA). The phospholipid mixture resembling the membrane of lung tissue pneumocytes (LPM) contained EPC/BPI/BPS/SM/TPE/Chol at a molar percentage of 27.7:7.5:10.5:9.4:26.2:18.7.[46] The phospholipid and peptide concentration were measured by methods described previously.[47,48]

Membrane Leakage Measurement. LUVs with a mean diameter of 0.1 μm were prepared as indicated above in buffer containing 10 mM Tris, 20 mM NaCl, pH 7.4, and CF at a concentration of 40 mM. Non-encapsulated CF was separated from the vesicle suspension through a Sephadex G-75 filtration column (Pharmacia, Uppsala, Sweden) eluted with buffer containing 10 mM Tris, 100 mM NaCl, and 1 mM EDTA, pH 7.4. Membrane rupture (leakage) of intraliposomal CF was assayed by treating the probe-loaded liposomes (final lipid concentration, 0.125 mM) with the appropriate amounts of peptide on microtiter plates using a microplate reader (FLUOstar; BMG Labtech, Offenburg, Germany), stabilized at 25 °C with the appropriate amounts of peptide, each well containing a final volume of 170 μL. The medium in the microtiter plates was continuously stirred to allow the rapid mixing of peptide and vesicles. Leakage was assayed until no more change in fluorescence was obtained. Fluorescence was measured using a Varian Cary Eclipse spectrofluorimeter. For details, see references 49 and 50.

Inner-Monolayer Phospholipid-Mixing (Fusion) Measurement. Peptide-induced phospholipid mixing of the inner monolayer was measured by resonance energy transfer.[51] This assay is based on the decrease in resonance energy transfer between two probes (NBD-PE and RhB-PE) when the lipids of the probe-containing vesicles are allowed to mix with lipids from vesicles lacking the probes. The concentration of each of the fluorescent probes within the liposome membrane was 0.6% mol. LUVs with a mean diameter of 0.2 μm were prepared as described above. LUVs were treated with sodium dithionite to completely reduce the NBD-labeled phospholipid located at the outer monolayer of the membrane. The final concentration of sodium dithionite was 100 mM (from a stock solution of 1 M dithionite in 1 M Tris, pH 10.0) and incubated for approximately 1 h on ice in the dark. Sodium dithionite was then removed by size exclusion chromatography through a Sephadex G-75 filtration column (Pharmacia, Uppsala, Sweden) eluted with buffer containing 10 mM Tris, 100 mM NaCl, and 1 mM EDTA, pH 7.4. The proportion of labeled and unlabeled vesicles, lipid concentration, and other experimental and measurement conditions were the same as indicated previously.[50]

Liposome Aggregation. LUVs with a mean diameter of 0.2 μm were prepared in buffer containing 10 mM Tris, 0.1 M NaCl, and 1 mM EDTA. Peptide-induced vesicle aggregation was detected by monitoring the optical density at 405 nm on a 96-well Anthos spectrometer. All measurements were performed at room temperature on microtiter plates, each well containing a final volume of 150 μL. The lipid concentration was 0.27 mM in all experiments, and the measured optical density was corrected for dilution upon peptide addition. The absorbance value for the vesicle suspension with the peptide was normalized according to the initial absorbance value of the vesicle suspension without peptide.

Peptide Binding to Vesicles. The partitioning of the peptide into the phospholipid bilayer was monitored by the fluorescence enhancement of tryptophan. Fluorescence spectra were recorded in an SLM Aminco 8000C spectrofluorometer with excitation and emission wavelengths of 290 and 348 nm, respectively, and 4 nm spectral bandwidths. Measurements were carried out in 20 mM HEPES, 50 mM NaCl, and 0.1 mM EDTA, pH 7.4.

Intensity values were corrected for dilution, and the scatter contribution was derived from lipid titration of a vesicle blank. Partitioning coefficients were obtained using[52]

$$\frac{I}{I_0} = 1 + \left(\frac{I_{max}}{I_0} - 1\right)\left(\frac{k[L]}{[W] + k[L]}\right)$$

where k is a mole fraction partition coefficient that represents the amount of peptide in the bilayers as a fraction of the total peptide present in the system, I_{max} is a variable value for the fluorescence enhancement at complete partitioning determined by fitting the equation to the experimental data, [L] is the lipid concentration, and [W] is the concentration of water (55.3 M).

Acrylamide Quenching of Trp Emission. For acrylamide quenching assays, aliquots from a 4 M solution of the water-soluble quencher were added to the solution-containing peptide in the presence and absence of liposomes at a peptide/lipid molar ratio of 1:100. The results obtained were corrected for dilution, and the scatter contribution was derived from acrylamide titration of a vesicle blank. The data were analyzed as previously described.[49]

Fluorescence Quenching by Lipophilic Probes. Quenching studies with lipophilic probes were performed by successive addition of small amounts of 5NS or 16NS in ethanol to the samples of the peptide incubated with LUV. The final concentration of ethanol was kept below 2.5% (v/v) to avoid any significant bilayer alterations. After each addition, an incubation period of 15 min was maintained before the measurement. The excitation and emission wavelengths were 290 and 348 nm, respectively. The data were analyzed as it has been described previously.[49]

Steady-State Fluorescence Anisotropy. MLVs were formed in 20 mM HEPES, 50 mM NaCl, and 0.1 mM EDTA, pH 7.4. Aliquots of TMA-DPH or DPH in *N*,*N*′-dimethylformamide were directly added into the lipid dispersion to obtain a probe/lipid molar ratio of 1/500. Samples were incubated for 15 or 60 min when TMA-DPH or DPH was used, respectively, 10 °C above the gel-to-liquid-crystalline phase transition temperature T_m of the phospholipid mixture. Afterward, the peptides were added to obtain a peptide/lipid molar ratio of 1/15 and were incubated 10 °C above the T_m of each lipid for 1 h, with occasional vortexing. All fluorescence studies were carried out using 5 mm × 5 mm quartz cuvettes in a final volume of 400 μL (315 μM lipid concentration). The steady-state fluorescence anisotropy, $\langle r \rangle$, was measured with an automated polarization accessory using a Varian Cary Eclipse fluorescence spectrometer, coupled to a Peltier for automatic temperature change, as described previously.[49]

Infrared Spectroscopy. Approximately 25 μL of a pelleted sample in D_2O were placed between two CaF_2 windows separated by 56-μm thick Teflon spacers in a liquid demountable cell (Harrick, Ossining, NY). The spectra were obtained in a Bruker IFS55 spectrometer using a deuterated triglycine sulfate detector. Each spectrum was obtained by collecting 200 interferograms with a nominal resolution of 2 cm^{-1}, transformed using triangular apodization, and, in order to average background spectra between sample spectra over the same time period, a sample shuttle accessory was used to obtain sample and background spectra. The spectrometer was continuously purged with dry air at a dew point of −40 °C in order to remove atmospheric water vapor from the bands of interest. All samples were equilibrated at the lowest temperature for 20 min before acquisition. An external bath circulator, connected to the infrared spectrometer, controlled the sample temperature. For temperature studies, samples were scanned using 2 °C intervals and a 2-min delay between each consecutive scan. Subtraction of buffer spectra taken at the same temperature as that of the samples was performed interactively using either GRAMS/32 or Spectra-Calc (Galactic Industries, Salem, MA) as described previously.[57,58] Frequencies at the center of gravity, when necessary, were measured by taking the top 10 points of each specific band and fitting them to a Gaussian band. The criterion used for buffer subtraction in the C═O and amide regions was the removal of the band near 1210 cm^{-1} and a flat baseline between 1800 and 2100 cm^{-1}. Band-narrowing strategies were applied to resolve the component bands in the Amide I′ region as previously reported.[59] Peptide secondary structure elements were quantified from a curve-fitting analysis by band decomposition of the original Amide I′ band after spectral smoothing (for details, see references 49 and 59).

Results

Recently, the existence of different membranotropic regions in the SARS-CoV Spike glycoprotein has been shown by using a peptide library encompassing the full sequence of the envelope glycoprotein,[39] which includes a highly hydrophobic aromatic domain similar to other Class I fusion membrane proteins.[39,40] Since this region could be important in the membrane fusion process,[5] we present here the results of the study of the interaction of a peptide derived from this region, SARS-CoV PTM, contiguous to the putative transmembrane domain, with model membranes (Figure 1).

The ability of the SARS-CoV PTM peptide to interact with membranes was determined from fluorescence studies of its three Trp residues in the presence of model membranes containing different phospholipid compositions at different lipid/peptide ratios.[62] The Trp fluorescence intensity of the SARS-CoV PTM peptide increased upon increasing the lipid/peptide ratio, indicating a significant change in the environment of the Trp moieties of the peptide (Figure 2A). The change on the Trp fluorescence of the peptide has allowed us to obtain its partition coefficient, K_p. $K_p$values in the range 10^4-10^5 were obtained for the different phospholipid compositions studied (Table 1), indicating that the peptide was bound to the membrane surface with high affinity. Similar K_p values have been found for other peptides in the presence of model membranes.[56−58,62] Higher K_p values were obtained for negatively charged phospholipid-containing bilayers and for EPC-containing liposomes (i.e., without cholesterol) than those corresponding to liposomes containing SM and TPE as well as for LPM and LE liposomes (Table 1). These results were further corroborated by the displacement in the emission frequency maximum of Trp in the presence of phospholipid LUVs. In solution, the peptide had an emission maximum at 347 nm when excited at the absorbance maximum, typical for Trp in a polar environment, whereas, in the presence of increasing concentrations of liposomes, the emission maximum of the Trp presented a shift of about 6−10 nm to lower wavelengths, implying that Trp sensed a low-polarity environment (entered in a hydrophobic environment) upon interaction with the membrane.

To investigate the accessibility of the Trp residues of the SARS-CoV PTM peptide to the aqueous phase in the presence of membranes having different phospholipid compositions, we used acrylamide, a neutral, water-soluble, highly efficient quenching probe. Stern−Volmer plots for the quenching of Trp by acrylamide, recorded in the absence and presence of lipid vesicles, are shown in Figure 2B. Linear Stern−Volmer plots are indicative of all Trp residues being accessible to acrylamide,

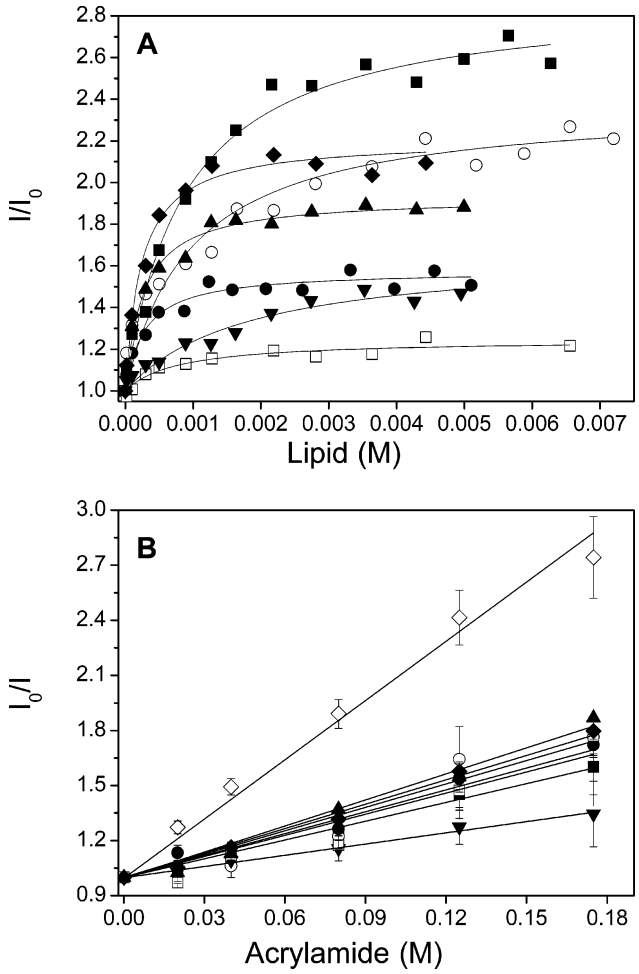

Figure 2. Change on the tryptophan fluorescence of the SARS-CoV PTM peptide in the presence of increasing lipid concentrations (A), acrylamide quenching studies of the tryptophan fluorescence of the peptide in aqueous solution (◇) and in the presence of LUVs having different lipid compositions (B). The lipid compositions used were EPC/BPI/CHOL at a molar ratio of 5:1:3 (▲), EPC/BPS/CHOL at a molar ratio of 5:4:1 (●), the LPM mixture (▼), the LE mixture (□), EPC (♦), EPC/TPE/CHOL at a molar ratio of 2:1:1 (○), and EPC/SM/CHOL at a molar ratio of 5:1:1 (■).

and, in all cases, the quenching of the peptide Trp residues showed acrylamide-dependent concentration behavior. In aqueous solution, the Trp residues of the peptide were exposed to the solvent allowing for a more efficient quenching. However, in the presence of the phospholipid membranes, the quenching effect was smaller, indicating that the Trp residues of the peptide were poorly accessible to the aqueous phase, suggesting that the peptide was effectively incorporated into the membranes. This is demonstrated by the lower K_{sv} values obtained from the corresponding Stern−Volmer plots (about 2−5 M^{-1}) compared to the K_{sv} value of about 11 M^{-1} obtained for the peptide in solution (Table 1).

The transverse location (penetration) of the SARS-CoV PTM peptide into the lipid bilayer was further investigated by monitoring the relative quenching of the fluorescence of the Trp residues by the lipophilic spin probes 5NS and 16NS when the peptide was incorporated in the fluid phase of vesicles having different phospholipid compositions (Figure 3). These two derivatized fatty acids differ in the position of the quencher moiety along the hydrocarbon chain and permit one to establish the depth of the peptide in the membrane by comparing the quenching results obtained with each of them. 5NS is a better quencher for molecules near or at the interface, while 16NS is a better probe for molecules buried deeply in the membrane. The variation of the fluorescence intensity with the increment of the effective concentration of both 5NS and 16NS probes is shown in Figure 3, along with the fitting lines obtained using eq 6, whereas the K_{sv} values for 5NS and 16NS are presented in Table 1. It can be seen that, in general, 16NS quenches the SARS-CoV PTM peptide fluorescence less efficiently than 5NS. Quenching depends on phospholipid composition, since the peptide is better quenched by 5NS in model membranes composed of EPC/TPE/Chol and the complex mixtures LE and LPM. However, model membranes composed of EPC, EPC/BPS/Chol, EPC/SM/Chol, or EPC/BPI/Chol present a lower quenching efficiency for both probes, which would indicate that the Trp residues are located at the membrane surface.

In order to explore the effect of the SARS-CoV PTM peptide in the destabilization of membrane vesicles, we studied their effect on the release of encapsulated fluorophores in model membranes made up of various compositions. The extent of leakage observed at different peptide to lipid molar ratios and the effect on different phospholipid compositions is shown in Figure 4A. It is interesting to note that the SARS-CoV PTM peptide induced a high percentage of leakage (leakage values between 85 and 100%), even at high lipid/peptide ratios as 30:1, for liposomes containing EPC, Chol, and/or SM (Figure 4A). Lower leakage values were obtained for liposomes composed of EPC alone, those containing BPI and BPS, and those composed of the complex phospholipid mixtures LE and LPM (40% and 25% leakage values were was observed at a peptide-to-lipid ratio of 1:10). The lowest leakage value was found for liposomes containing TPE, which, at the highest peptide-to-lipid ratio studied, i.e., 1:10, only about 12% leakage was attained (Figure 4A). The induction of inner-monolayer lipid mixing (fusion) by the SARS-CoV PTM peptide, as a measure of its fusogenic activity, was tested with several types of vesicles utilizing the probe dilution assay,[51,63] and the results are shown

TABLE 1: Partition Coefficients and Stern−Volmer Quenching Constants for the SARS CoV PTM Peptide in Buffer and Incorporated in LUVs of Different Compositions

LUV compositions	K_P	$\Delta\lambda^a$ (nm)	K_{sv} (M^{-1}) acrylamide	K_{sv} (M^{-1}) 5-NS	K_{sv} (M^{-1}) 16-NS
EPC	$2.33 \pm 0.43 \times 10^5$	8	4.47	1.37	1.94
EPC/SM/CHOL 5:1:1	$6.26 \pm 0.67 \times 10^4$	10	3.42	3.10	2.87
EPC/TPE/CHOL 2:1:1	$5.61 \pm 0.75 \times 10^4$	8	4.3	9.34	2.20
EPC/BPS/CHOL 5:4:1	$1.93 \pm 0.67 \times 10^5$	7	4.08	1.33	1.74
EPC/BPI/CHOL 5:1:3	$2.06 \pm 0.46 \times 10^5$	6	4.68	6.60	5.96
LPM	$7.04 \pm 0.62 \times 10^4$	7	2.05	7.66	2.70
LE	$3.06 \pm 0.40 \times 10^4$	10	3.87	5.87	3.50
SARS-CoV PTM in buffer			10.58		

[a] $\Delta\lambda$ corresponds to a peptide/lipid ratio of 1:300.

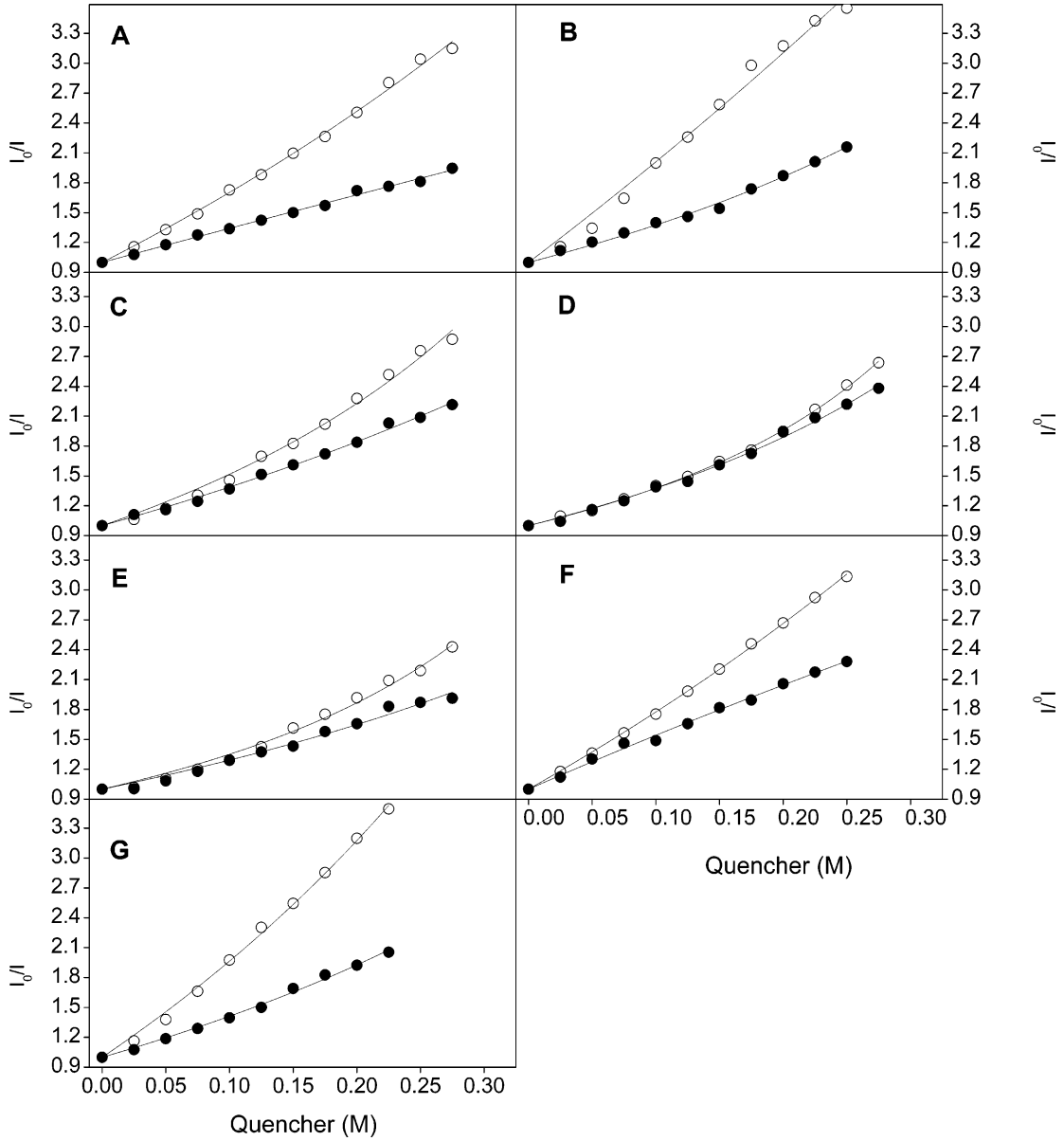

Figure 3. 5NS (○) and 16NS (●) quenching of Trp fluorescence of the SARS-CoV PTM peptide in the presence of LUVs for different lipid compositions. The lipid compositions used were (A) LE, (B) EPC/TPE/CHOL at a molar ratio of 2:1:1, (C) EPC/SM/CHOL at a molar ratio of 5:1:1, (D) EPC, (E), EPC/BPS/CHOL at a molar ratio of 5:4:1, (F) EPC/BPI/CHOL at a molar ratio of 5:1:3, and (G) LPM.

in Figure 4B. The higher fusion values were found for liposomes containing negatively charged phospholipids (liposomes containing BPI and BPS) as well as the complex LPM mixture (which also contains negatively charged phospholipids), which showed fusion values between 40 and 60%. Lower fusion values were observed for liposomes containing either SM and Chol or Chol (about 25% and 20% fusion, respectively). The other compositions studied showed fusion values lower than 10% (Figure 4B). The ability of the SARS-CoV PTM peptide to induce vesicle aggregation was tested in order to investigate whether this property correlated with peptide−membrane interaction as commented above. The changes in the absorbance of different liposome compositions as a function of the peptide-to-lipid molar ratio are shown in Figure 4C. It is interesting to note that the presence of negatively charged phospholipids in the liposomes favored the aggregation process, increasing more than 3 times the o.d. A similar effect was also found for the LPM complex mixture in comparison with the other liposome compositions. Lower aggregation values were obtained for the other liposomes tested. Significantly, the effect of the SARS-CoV PTM peptide on the fusion values for the different membrane mixtures coincides with what has been observed in the aggregation assays (Figure 4C).

The effect of the SARS-CoV PTM peptide on the structural and thermotropic properties of phospholipid membranes was investigated by measuring the steady-state fluorescence anisotropy of the fluorescent probes DPH and TMA-DPH incorporated into model membranes composed of saturated synthetic phospholipids as a function of temperature (Figure 5). DPH and its derivatives are very useful fluorescent probes for monitoring the organization and dynamics of membranes, since fluorescence polarization is correlated to the rotational diffusion of membrane-embedded probes, itself sensitive to the packing of the fatty acyl chains.[64] These probes differ in their orientation and location in the membrane, so that it was possible to analyze the effect of the SARS-CoV PTM peptide on the structural and thermotropic properties along the full length of the palisade structure of the membrane, since DPH is known to partition mainly into the hydrophobic core of the membrane, whereas TMA-DPH is oriented at the membrane bilayer with its charge

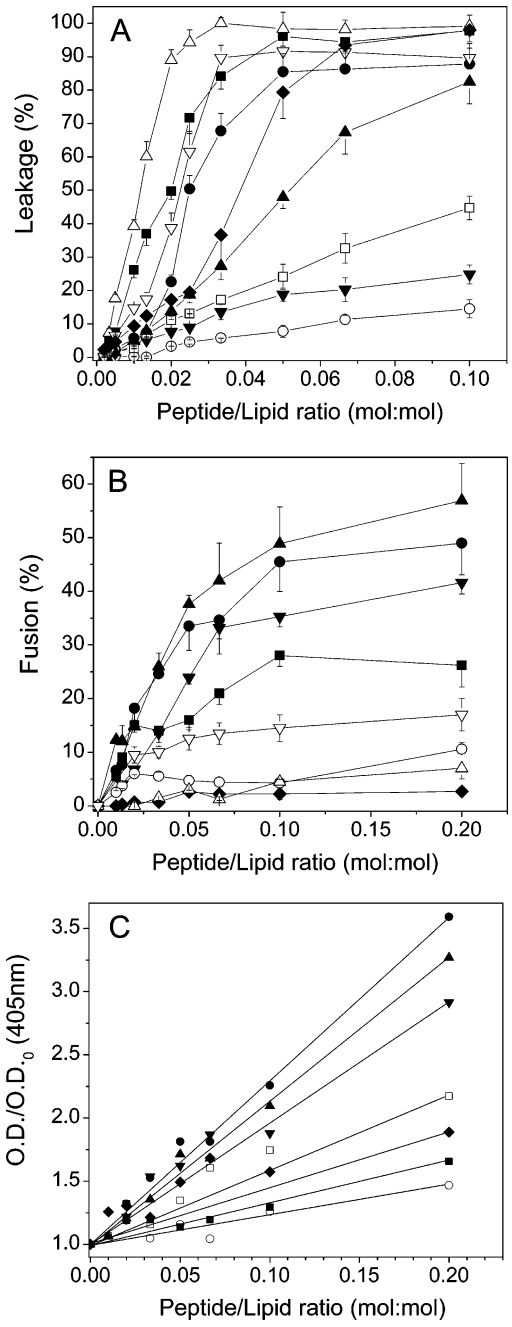

Figure 4. Effect of the SARS-CoV PTM peptide on (A) membrane rupture, i.e., leakage, (B) membrane lipid mixing of the inner monolayer, i.e., fusion, and (C) aggregation of LUVs having different lipid compositions at different peptide-to-lipid molar ratios. The lipid compositions used were EPC/SM 5:1 (△), EPC/BPS/CHOL at a molar ratio of 5:4:1 (●), EPC (♦), EPC/SM/CHOL at a molar ratio of 5:1:1 (■), EPC/CHOL at a molar ratio of 5:1 (▽), EPC/BPI/CHOL at a molar ratio of 5:1:3 (▲), the LPM mixture (▼), the LE mixture (□), and EPC/TPE/CHOL at a molar ratio of 2:1:1 (○). In panel C, the lines connecting the experimental data are merely guides to the eye.

localized at the lipid−water interface.[64−66] The SARS-CoV PTM peptide decreased the cooperativity of the transition as observed by both types of probes, as well as induced an increase of the anisotropy for DPH of about 0.02 anisotropy units both below and above the gel-to-liquid-crystalline transition T_m of DMPC, but only 0.015 anisotropy units below the T_m for TMA-DPH, suggesting that the peptide was able to decrease the mobility of the phospholipid acyl chains when compared to the pure phospholipid (Figures 5A and 5B). In the case of DMPS, a similar decrease in cooperativity was observed, concomitantly with a shift of T_m of approximately 3−4 °C to lower temperatures (Figures 5C and 5D). For vesicles composed of DMPG, the SARS-CoV PTM peptide decreased the cooperativity of the transition, as well as it increased the anisotropy above T_m by 0.03−0.04 anisotropy units (Figures 5E and 5F), although an increase and a decrease of about 0.02 anisotropy units above and below T_m was observed for TMA-DPH. These differences could suggest that the difference in charge between DMPC, DMPS, and DMPG could affect the effects of the peptide incorporation into the membrane. When vesicles composed of POPE were studied, no effect was observed when DPH was used, but the PTM peptide decreased the anisotropy of TMA-DPH at all temperatures by 0.03−0.04 anisotropy units (Figure 5G,H). Moreover, when the PTM peptide was incorporated into DMPA-containing vesicles, neither the cooperativity nor the anisotropy below and above the T_m of the mixture was affected (Figure 5I,J). Taking into account these results together with the ones mentioned above, it could be suggested that the SARS-CoV PTM peptide, although interacting with the membrane, should be located at the lipid−water interface.[57]

The existence of structural changes on the SARS-CoV PTM peptide induced by membrane binding has been studied by looking at the infrared Amide I′ band located between 1700 and 1600 cm^{-1}. The infrared spectrum of the Amide I′ region of the fully hydrated peptide in D_2O buffer at different temperatures is shown in Figure 6A. The spectrum was formed by different underlying components that gave place to a broad and asymmetric band whose frequency maximum changed as the temperature increased: whereas, at low temperatures, the maximum of the band was located at about 1630 cm^{-1}, at high temperatures, two bands were apparent, a broad band at about 1647 cm^{-1} and a narrow one at about 1626 cm^{-1} (Figure 6A). Whereas the broad band at about 1647 cm^{-1} corresponds to a mixture of unordered and helical structures,[67] the narrow band at about 1626 cm^{-1} corresponds to either β-sheet structures or self-aggregated peptides, forming a intermolecular network of hydrogen-bonded β-structures or both.[68] The infrared spectra in the Amide I′ region of the SARS-CoV PTM peptide in the presence of DMPC, DMPG, and DMPA at phospholipid/peptide molar ratios of 15:1 are shown in Figure 6B−D, respectively. What is indeed significant is that the Amide I′ region of the SARS-CoV PTM peptide in the presence of either DMPC or DMPG, taken at temperatures above and below the main phase transition temperature T_m of each specific phospholipid, was different. Outstandingly, the change in frequency of the Amide I′ band took place at the same temperature as that at which the phase transition of DMPC and DMPG occurred, as observed by the shift of the C═O stretching maximum with temperature (Figure 6E,F); however, the observed change in frequency was different in the presence of each phospholipid since the frequency maximum of the Amide I′ band of the peptide in the presence of DMPC decreased as the temperature increased, and the opposite was true in the presence of DMPG (Figures 6E,F). It is interesting to note that the bandwidth at half-height of the Amide I′ band envelope when the peptide was bound to the membranes decreased about 3−4 cm^{-1} compared to the peptide in solution, indicating either the presence of additional structures contributing to the broader envelope for the peptide in solution or a different flexibility of the peptide or both. In contrast, the Amide I′ envelope band of the SARS-CoV PTM peptide in the presence of DMPA presented a maximum at about 1626−1627 cm^{-1} at all temperatures studied (Figure 6D,G). These data suggest that the SARS-CoV PTM peptide has different second-

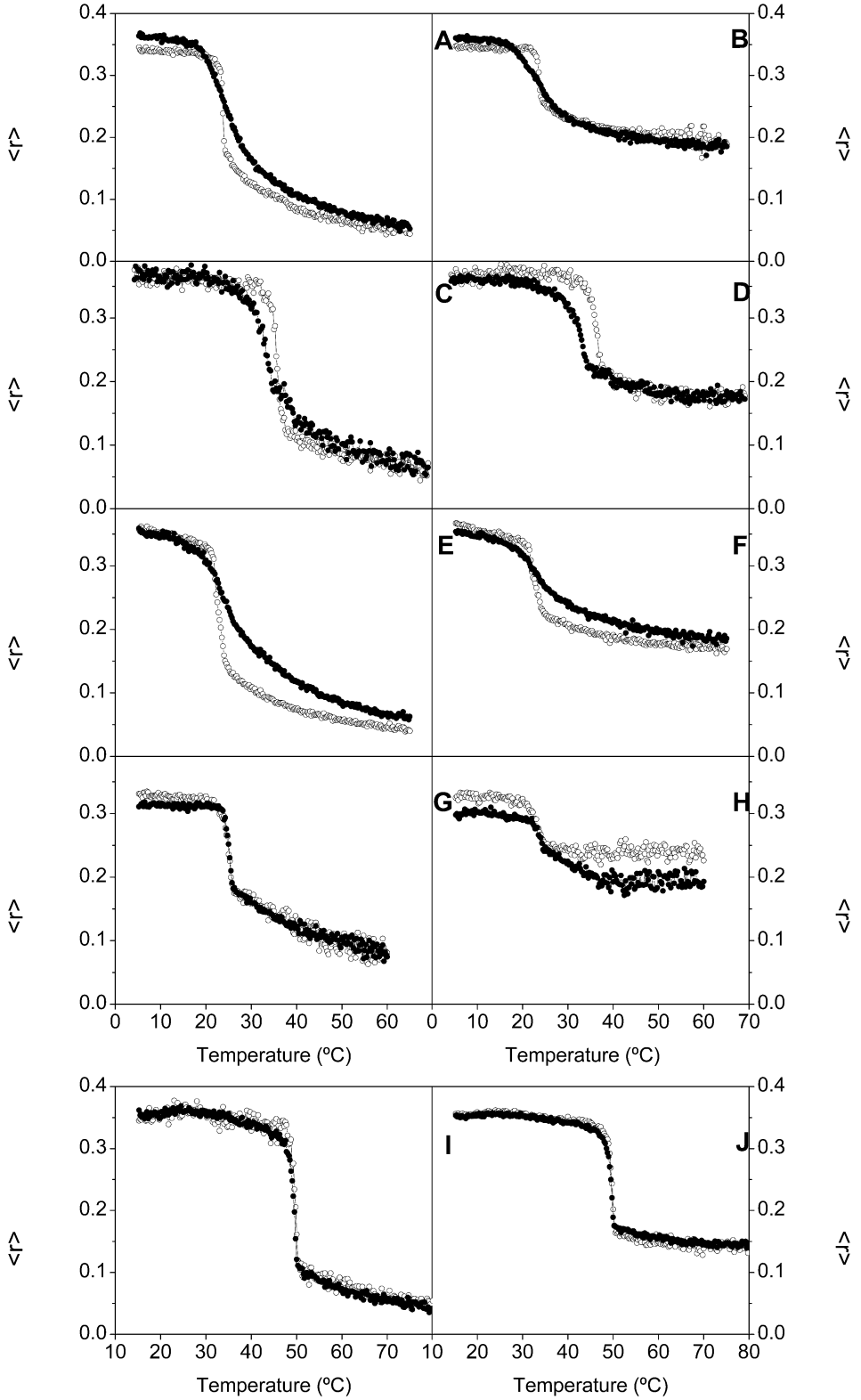

Figure 5. Anisotropy values, $\langle r \rangle$, of DPH (A,C,E,G,I) and TMA-DPH (B,D,F,H,J) fluorescent probes in model membranes composed of (A,B) DMPC, (C,D) DMPS, (E,F) DMPG, (G,H) POPE, and (I,J) DMPA as a function of temperature. Data correspond to vesicles in the absence (○) and in the presence (●) of the SARS-CoV PTM peptide.

ary structures in the presence of different phospholipid types and phases (see below).

To assign the component bands to specific structural features and estimate the percentage of each component, we have decomposed the Amide I′ infrared band as described in the Materials and Methods section and compared them to literature values.[57,58,68] For the peptide in solution, we have identified different component bands at frequencies of about 1678, 1662, 1648, 1635, 1627, and 1612 cm^{-1} (Figure 7A). It is also possible to distinguish different component bands having similar frequencies as those found for the peptide in the presence of DMPC, DMPG, and DMPA (Figure 7B−D). The number and frequencies of the Amide I′ component bands for these samples were similar to those found for the peptide in solution, but their intensity varied. To assign the component bands to specific structural features and estimate the percentage of each compo-

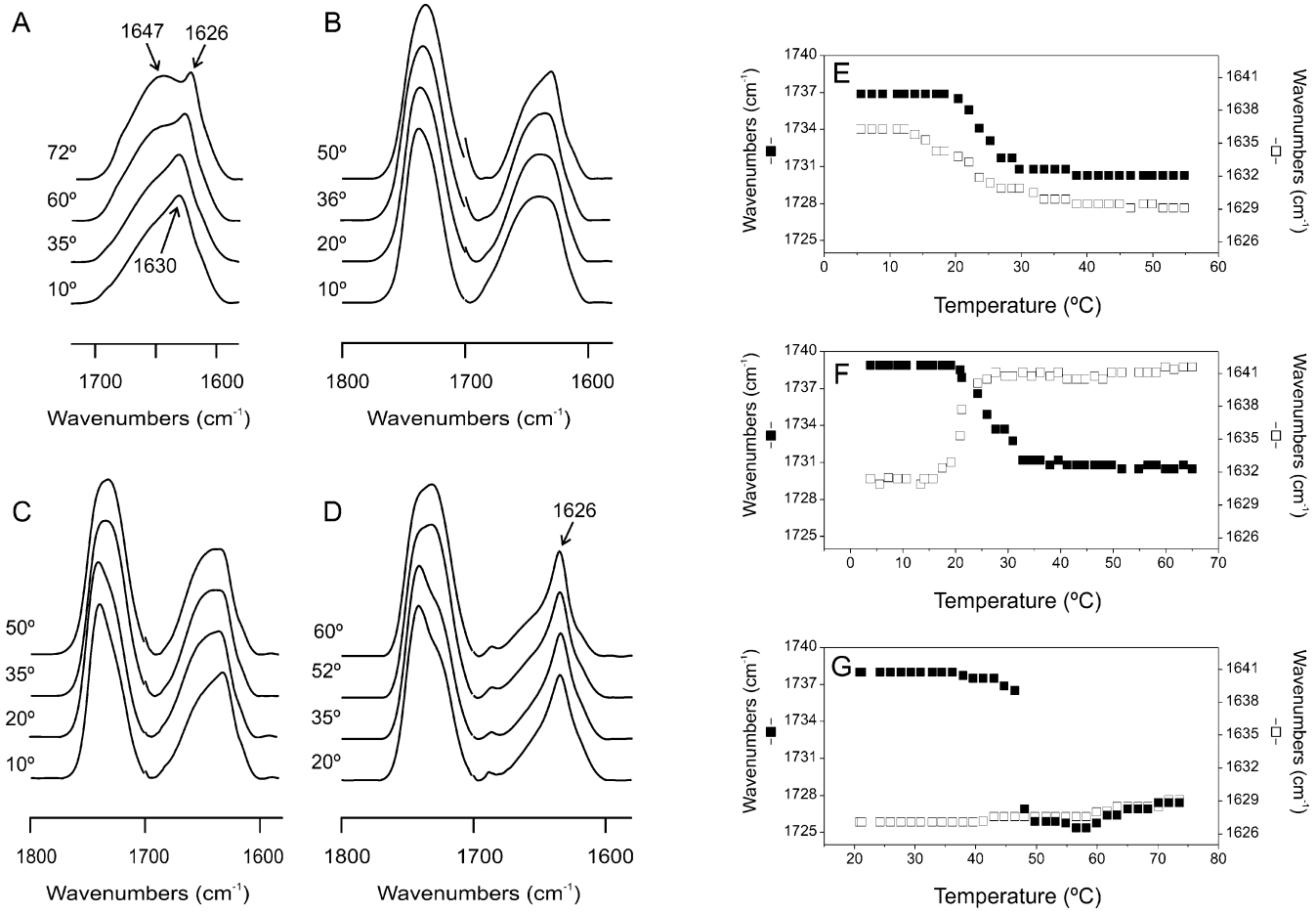

Figure 6. Stacked infrared spectra of the Amide I′ and C═O regions for samples containing the SARS-CoV PTM peptide in solution (A) and in the presence of DMPC (B), DMPG (C), and DMPA (D) at different temperatures as indicated. Also shown is the temperature dependence of the frequency maximum of the phospholipid C═O symmetric stretching (■) and the peptide Amide I′ (□) bands for samples containing the SARS-CoV PTM peptide and (E) DMPC, (F) DMPG, and (G) DMPA. The phospholipid-to-peptide molar ratio was 15:1.

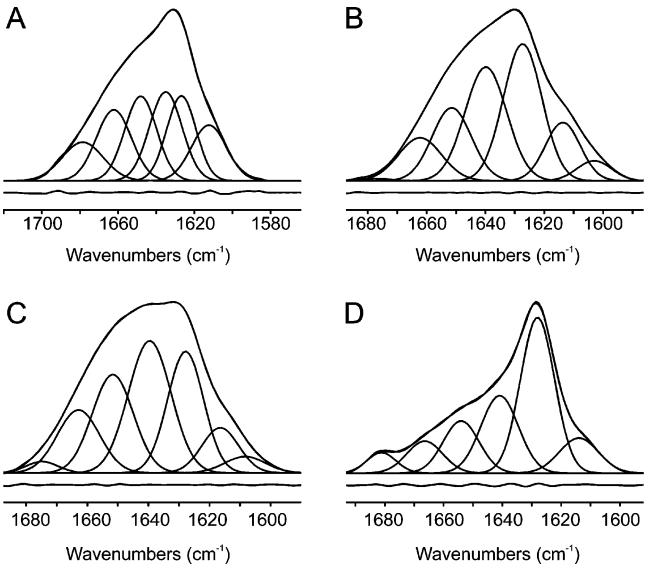

Figure 7. Amide I′ band decomposition of the SARS-CoV PTM peptide in aqueous solution (A) and in the presence of DMPC (B), DMPG (C), and DMPA (D). The spectra were taken at 10 °C above the phospholipid T_m and 35 °C for the peptide in solution. The component bands, the original envelope, and the difference between the fitted curve and the original spectrum are shown.

nent, we have decomposed the Amide I′ infrared band as described previously.[62] Bands below 1620 cm^{-1} are outside the range of frequencies usually observed for the secondary structure elements of proteins, so they were not considered in the determination of the total area of the Amide I′ band.[58,62,68,69] The most significant difference between the secondary structure of the SARS-CoV PTM peptide in solution and in the presence of either DMPC or DMPG is that, in the latter cases, a significant decrease in β-sheet (36% and 26%, respectively, compared with 44% in solution) and β-turn (0% and 2%, respectively, compared with 13% in solution) structures were observed, concomitantly with an increase of α-helix and/or random coil (64% and 72%, respectively, compared with 43% in solution). However, in the presence of DMPA, a slight increase in α-helix and/or random coil (50%) was observed as well as a slight decrease in β-turn (5%) when compared with the peptide in solution. It should be recalled that two bands at 1626 and 1635 cm^{-1} appeared for the protein in solution, but only one intense band at 1628 cm^{-1} appeared for the peptide in the presence of DMPA. These results imply that the secondary structure of the SARS-CoV PTM peptide was affected by phospholipid composition.

Discussion

Viruses attach to cells through different mechanisms, but there is only one way to get into the host cell through the membrane: viral and host-cell membrane fusion supported by membrane fusion proteins. The membrane fusion protein of SARS-CoV is the envelope Spike glycoprotein, and it is thought, similarly to other Class I membrane fusion proteins, that several trimers of the S protein are capable of juxtaposing, destabilizing,

and merging the viral and cellular membranes so that a fusion pore is formed.[1,3,5,25,40,52,70,71] Therefore, membrane fusion can be described as a succession of different steps, namely, apposition of membranes, hemifusion of the outer leaflets to form a stalk, fusion pore formation through merging of both bilayers at the stalk point, and, finally, fusion pore enlargement with full contents mixing.[24,72] A lot of research on membrane fusion proteins point out that there are several regions within these proteins that are involved in the fusion process, and are decisive for membrane fusion to take place.[34,37,39,40,50,52,58,71,73−75] Destabilization of the lipid bilayer and membrane fusion appears then to be the result of the binding and interaction of these segments with the biological membranes. However, little is known about how the complex series of protein/protein and protein/phospholipid interactions drive membrane apposition and how they overcome the energy barriers for membrane fusion. On the basis of our recent work,[39] we have selected a highly aromatic domain from the SARS-CoV pre-transmembrane sequence, also found in other Class I fusion membrane proteins, to carry out a biophysical study, aiming to elucidate the capacity of this region adjacent to the transmembrane domain of the protein, to interact and disrupt membranes with an approach based on different but complementary strategies.

The SARS-CoV PTM peptide studied in this work partitions with high affinity to model membranes having different phospholipid compositions. We and others have previously found similar binding affinities for other peptides pertaining to other membrane fusion proteins, as reported previously.[56−58,62,76,77] However, the degree of partitioning of the SARS-CoV PTM peptide had no specificity for any particular lipid composition, as it has also been found for other peptides. This was further demonstrated by hydrophilic (acrylamide) and lipophilic (NS) probe quenching, suggesting that the SARS-CoV PTM peptide was effectively incorporated into the membranes but located at the membrane interface. The SARS-CoV PTM peptide was also capable of altering membrane stability, causing the release of fluorescent probes. However this effect was dependent on lipid composition and on the lipid/peptide molar ratio, with the highest effect being observed for liposomes containing EPC, Chol, and/or SM. Lower but significant values were observed for liposomes composed of EPC alone, those containing BPI and BPS, as well as those composed of the complex phospholipid mixtures LE and LPM. The observed effect should therefore be due primarily to hydrophobic interactions within the bilayer but not to the specific charge of the phospholipid headgroups. The binding to the surface and the modulation of the phospholipid biophysical properties, which take place when the peptide is bound to the membrane, i.e., partitioning into the membrane surface and perturbation of the bilayer architecture, could be related to the conformational changes that might occur during the activity of the SARS-CoV Spike protein. The induction of fusion by the SARS-CoV PTM peptide was also studied, and a similar result was obtained, since significant membrane fusion values were found in the presence of liposomes composed of negatively charged phospholipids as well as for the complex lipid mixtures studied (vide supra).

The differences we have found on the effect produced by the PTM peptide on leakage and fusion, i.e., higher aggregation and fusion values but lower leakage values in the presence of negatively charged phospholipids, and the opposite for the other types of phospholipids studied here, might indicate the possibility that negatively charged phospholipids (it should be recalled that type 1 and 2 lung pneumocytes are the most important cell targets of SARS-CoV, and their plasma membranes contain PI and PS among other phospholipids) could play an important role and stimulate the first step in the fusion process, i.e., approximation and binding of the protein to the membrane, whereas the ensuing destabilization would be induced by the presence of other phospholipid types.

We have shown that the SARS-CoV PTM peptide is capable of affecting the steady-state fluorescence anisotropy of fluorescent probes located in the palisade structure of the membrane, since it decreased the cooperativity of the transition, as observed by both types of probes for the phospholipids DMPC, DMPG, and DMPS. Therefore, the peptide was able to decrease the mobility of the phospholipid acyl chains when compared to the pure phospholipid. However, some differences were found related to the anisotropy change below and above the T_m of the pure phospholipid, suggesting that the difference in charge between DPMC, DMPS, and DMPG could affect the effects of the incorporation of the peptide into the membrane. It is interesting to note that the peptide did not induce any significant effect on either the cooperativity or the anisotropy of DMPA, which, similarly to DMPG and DMPS, bears a negative charge in its headgroup. These data suggest, as commented above, that the SARS-CoV PTM peptide, although interacting with the membrane, should be located at the lipid−water interface.[57]

The infrared spectra of the Amide I′ region of the fully hydrated peptide changed with temperature, indicating a low stability of its conformation, where the β-sheet structure predominated. However, we have observed differences in the proportion of the different secondary elements when the peptide was incorporated into membranes of different phospholipid composition, since its conformation changed depending on phospholipid composition. Whereas the α-helix, β-sheet, and random percentages were similar in solution and in the presence of DMPA, they changed significantly in the presence of DMPC and DMPG, which would be in accordance with the fluorescence data commented above. Interestingly, the β-turn content decreased in the presence of all types of phospholipids. These data would suggest that the presence of different phospholipid headgroups would modulate the secondary structure of the peptide as it has been suggested for other peptides.[57,58,62] It is interesting to note that the peptide in the presence of both DMPC and DMPG, but not in the presence of DMPA, changed its conformation concomitantly with the phospholipid gel-to-liquid-crystalline phase transition. The fact that peptide structure in DMPA remains unaltered is consistent with the effect observed in the TMA-DPH and DPH anisotropy experiments mentioned above. This effect suggests that, apart from a negative-charged phospholipid, the presence of a more sizable headgroup is important in the peptide−membrane interaction, perhaps permitting a greater hydration. It has been shown that, besides its fusogenic properties, the Trp-rich domain is also required for membrane fusion, perhaps by facilitating oligomerization of gp41[37] or stabilization of the spike trimer.[78] Membrane fusion is an energy-costing event that involves destabilization of the bilayer and dehydration of the interfacial regions.[23,24,79] The structural changes that take place when the SARS-CoV PTM peptide binds to the membrane could be indicative of the conformational change that takes place during the metastable (native) to stable (fusogenic) conformational changes of the SARS S glycoprotein following binding of the SARS envelope glycoprotein to its receptors. In the case of the peptide in DMPG, this effect is shown in the IR experiments. We can observe that a change from β-sheet structures or self-aggregated peptides to a mixture of unordered and helical structures takes place at the same temperature of DMPG. This change might be related to a

possible role of the peptide in the fusion process. In the first steps of fusion, the peptide would be able to facilitate the oligomerization/trimerization of the spike protein, and, subsequently, after membrane interaction, the conformational change would be an energy supplier to assist in the fusion process. This is consistent with the results obtained in the fusion and aggregation assays in which the SARS-CoV PTM peptide was more effective in promoting fusion in negatively charged membranes.

Conclusions

The SARS-CoV PTM peptide adopts different conformations when bound to membranes of different compositions, altering the physical properties of the phospholipid bilayer and inducing a very efficient release of trapped probes. Therefore, this region of the SARS Spike glycoprotein should play a significant role in the fusion mechanism, and, at the same time, it could be considered that this region of the protein during and/or after the fusion process could interact with other membranotropic regions and therefore might be essential for the assistance and enhancement of the viral and cell fusion process.

Abbreviations

16NS: 16-doxyl-stearic acid; 5NS: 5-doxyl-stearic acid; BPI: bovine brain L-α-phosphatidylinositol; BPS: bovine brain phosphatidylserine; CF: 5-carboxyfluorescein; Chol: cholesterol; CoV: coronavirus; DMPA: 1,2-dimyristoyl-*sn*-glycero-phosphatidic acid; DMPC: 1,2-dimyristoyl-*sn*-glycero-phosphatidylcholine; DMPG: 1,2-dimyristoyl-*sn*-glycero-phosphatidylglycerol; DMPS: 1,2-dimyristoyl-*sn*-glycero-3-phosphatidylserine; DPH: 1,6-diphenyl-1,3,5-hexatriene; EPC: egg yolk L-α-phosphatidylcholine; EPG: egg yolk L-α-phosphatidylglycerol; FP: fusion peptide; FTIR: Fourier-transform infrared spectroscopy; HIV-1: human immunodeficiency virus type 1; HR1: heptad repeat region 1; HR2: heptad repeat region 2; LE: lung extract; LPM: lung pneumocytes membrane; LUV: large unilamellar vesicles; MLV: multilamellar vesicles; NBD-PE: *N*-(7-nitrobenz-2-oxa-1,3-diazol-4-yl)-1,2-dihexadecanoyl-*sn*-glycero-3-phosphoethanolamine; POPE: 1-palmitoyl-2-oleoyl-*sn*-glycero-3-phosphoethanolamine; PTM: pre-transmembrane domain; RhB-PE: lissamine rhodamine B 1,2-dihexadecanoyl-*sn*-glycero-3-phosphoethanolamine; SARS: severe acute respiratory syndrome; SM: egg sphingomyelin; T_m: temperature of the gel-to-liquid-crystalline phase transition; TM: transmembrane domain; TMA-DPH: 1-(4-trimethylammoniumphenyl)-6-phenyl-1,3,5-hexatriene; TPE: egg transesterified L-α-phosphatidylethanolamine.

Acknowledgment. This work was supported by Grant BFU2005-00186-BMC (Ministerio de Ciencia y Tecnología, Spain) to J.V. M.R.M. and A.B. are recipients of a pre-doctoral fellowship from Ministerio de Educación, Cultura y Deporte, Spain. A.J.P. and J.G. are recipients of pre-doctoral fellowships from the Autonomous Government of the Valencian Community, Spain.

References and Notes

(1) Drosten, C.; Chiu, L. L.; Panning, M.; Leong, H. N.; Preiser, W.; Tam, J. S.; Gunther, S.; Kramme, S.; Emmerich, P.; Ng, W. L.; Schmitz, H.; Koay, E. S. *J. Clin. Microbiol.* **2004**, *42*, 2043.

(2) Peiris, J. S.; Lai, S. T.; Poon, L. L.; Guan, Y.; Yam, L. Y.; Lim, W.; Nicholls, J.; Yee, W. K.; Yan, W. W.; Cheung, M. T.; Cheng, V. C.; Chan, K. H.; Tsang, D. N.; Yung, R. W.; Ng, T. K.; Yuen, K. Y. *Lancet* **2003**, *361*, 1319.

(3) Ksiazek, T. G.; Erdman, D.; Goldsmith, C. S.; Zaki, S. R.; Peret, T.; Emery, S.; Tong, S.; Urbani, C.; Comer, J. A.; Lim, W.; Rollin, P. E.; Dowell, S. F.; Ling, A. E.; Humphrey, C. D.; Shieh, W. J.; Guarner, J.; Paddock, C. D.; Rota, P.; Fields, B.; DeRisi, J.; Yang, J. Y.; Cox, N.; Hughes, J. M.; LeDuc, J. W.; Bellini, W. J.; Anderson, L. J. *N. Engl. J. Med.* **2003**, *348*, 1953.

(4) Poutanen, S. M.; Low, D. E.; Henry, B.; Finkelstein, S.; Rose, D.; Green, K.; Tellier, R.; Draker, R.; Adachi, D.; Ayers, M.; Chan, A. K.; Skowronski, D. M.; Salit, I.; Simor, A. E.; Slutsky, A. S.; Doyle, P. W.; Krajden, M.; Petric, M.; Brunham, R. C.; McGeer, A. J. *N. Engl. J. Med.* **2003**, *348*, 1995.

(5) Yeung, K. S.; Yamanaka, G. A.; Meanwell, N. A. *Med. Res. Rev.* **2006**, *26*, 414.

(6) Li, W.; Moore, M. J.; Vasilieva, N.; Sui, J.; Wong, S. K.; Berne, M. A.; Somasundaran, M.; Sullivan, J. L.; Luzuriaga, K.; Greenough, T. C.; Choe, H.; Farzan, M. *Nature* **2003**, *426*, 450.

(7) Masters, P. S. *Adv. Virus Res.* **2006**, *66*, 193.

(8) Babcock, G. J.; Esshaki, D. J.; Thomas, W. D., Jr.; Ambrosino, D. M. *J. Virol.* **2004**, *78*, 4552.

(9) Wong, S. K.; Li, W.; Moore, M. J.; Choe, H.; Farzan, M. *J. Biol. Chem.* **2004**, *279*, 3197.

(10) Rota, P. A.; Oberste, M. S.; Monroe, S. S.; Nix, W. A.; Campagnoli, R.; Icenogle, J. P.; Penaranda, S.; Bankamp, B.; Maher, K.; Chen, M. H.; Tong, S.; Tamin, A.; Lowe, L.; Frace, M.; DeRisi, J. L.; Chen, Q.; Wang, D.; Erdman, D. D.; Peret, T. C.; Burns, C.; Ksiazek, T. G.; Rollin, P. E.; Sanchez, A.; Liffick, S.; Holloway, B.; Limor, J.; McCaustland, K.; Olsen-Rasmussen, M.; Fouchier, R.; Gunther, S.; Osterhaus, A. D.; Drosten, C.; Pallansch, M. A.; Anderson, L. J.; Bellini, W. J. *Science* **2003**, *300*, 1394.

(11) Xiao, X.; Chakraborti, S.; Dimitrov, A. S.; Gramatikoff, K.; Dimitrov, D. S. *Biochem. Biophys. Res. Commun.* **2003**, *312*, 1159.

(12) Xu, Y.; Zhu, J.; Liu, Y.; Lou, Z.; Yuan, F.; Liu, Y.; Cole, D. K.; Ni, L.; Su, N.; Qin, L.; Li, X.; Bai, Z.; Bell, J. I.; Pang, H.; Tien, P.; Gao, G. F.; Rao, Z. *Biochemistry* **2004**, *43*, 14064.

(13) Zhu, J.; Xiao, G.; Xu, Y.; Yuan, F.; Zheng, C.; Liu, Y.; Yan, H.; Cole, D. K.; Bell, J. I.; Rao, Z.; Tien, P.; Gao, G. F. *Biochem. Biophys. Res. Commun.* **2004**, *319*, 283.

(14) Tripet, B.; Howard, M. W.; Jobling, M.; Holmes, R. K.; Holmes, K. V.; Hodges, R. S. *J. Biol. Chem.* **2004**, *279*, 20836.

(15) Liu, S.; Xiao, G.; Chen, Y.; He, Y.; Niu, J.; Escalante, C. R.; Xiong, H.; Farmar, J.; Debnath, A. K.; Tien, P.; Jiang, S. *Lancet* **2004**, *363*, 938.

(16) Ingallinella, P.; Bianchi, E.; Finotto, M.; Cantoni, G.; Eckert, D. M.; Supekar, V. M.; Bruckmann, C.; Carfi, A.; Pessi, A. *Proc. Natl. Acad. Sci. U.S.A.* **2004**, *101*, 8709.

(17) Bosch, B. J.; van der Zee, R.; de Haan, C. A.; Rottier, P. J. *J. Virol.* **2003**, *77*, 8801.

(18) Bosch, B. J.; Martina, B. E.; Van Der Zee, R.; Lepault, J.; Haijema, B. J.; Versluis, C.; Heck, A. J.; De Groot, R.; Osterhaus, A. D.; Rottier, P. J. *Proc. Natl. Acad. Sci. U.S.A.* **2004**, *101*, 8455.

(19) Gallaher, W. R. *Cell* **1996**, *85*, 477.

(20) Chambers, P.; Pringle, C. R.; Easton, A. J. *J. Gen. Virol.* **1990**, *71* (Pt 12), 3075.

(21) Gallaher, W. R.; Ball, J. M.; Garry, R. F.; Griffin, M. C.; Montelaro, R. C. *AIDS Res. Hum. Retroviruses* **1989**, *5*, 431.

(22) Wilson, I. A.; Skehel, J. J.; Wiley, D. C. *Nature* **1981**, *289*, 366.

(23) Chernomordik, L. V.; Zimmerberg, J.; Kozlov, M. M. *J. Cell Biol.* **2006**, *175*, 201.

(24) Chernomordik, L. V.; Kozlov, M. M. *Cell* **2005**, *123*, 375.

(25) Blumenthal, R.; Clague, M. J.; Durell, S. R.; Epand, R. M. *Chem. Rev.* **2003**, *103*, 53.

(26) Earp, L. J.; Delos, S. E.; Park, H. E.; White, J. M. *Curr. Top. Microbiol. Immunol.* **2005**, *285*, 25.

(27) Peisajovich, S. G.; Shai, Y. *Biochim. Biophys. Acta* **2003**, *1614*, 122.

(28) Suarez, T.; Nir, S.; Goni, F. M.; Saez-Cirion, A.; Nieva, J. L. *FEBS Lett.* **2000**, *477*, 145.

(29) Saez-Cirion, A.; Gomara, M. J.; Agirre, A.; Nieva, J. L. *FEBS Lett.* **2003**, *533*, 47.

(30) Salzwedel, K.; West, J. T.; Hunter, E. *J. Virol.* **1999**, *73*, 2469.

(31) Munoz-Barroso, I.; Salzwedel, K.; Hunter, E.; Blumenthal, R. *J. Virol.* **1999**, *73*, 6089.

(32) Tong, S.; Yi, F.; Martin, A.; Yao, Q.; Li, M.; Compans, R. W. *Virology* **2001**, *280*, 52.

(33) Zhou, J.; Dutch, R. E.; Lamb, R. A. *Virology* **1997**, *239*, 327.

(34) Moreno, M. R.; Pascual, R.; Villalain, J. *Biochim. Biophys. Acta* **2004**, *1661*, 97.

(35) Suarez, T.; Gallaher, W. R.; Agirre, A.; Goni, F. M.; Nieva, J. L. *J. Virol.* **2000**, *74*, 8038.

(36) Saez-Cirion, A.; Nir, S.; Lorizate, M.; Agirre, A.; Cruz, A.; Perez-Gil, J.; Nieva, J. L. *J. Biol. Chem.* **2002**, *277*, 21776.

(37) Saez-Cirion, A.; Arrondo, J. L.; Gomara, M. J.; Lorizate, M.; Iloro, I.; Melikyan, G.; Nieva, J. L. *Biophys. J.* **2003**, *85*, 3769.

(38) Epand, R. F.; Sayer, B. G.; Epand, R. M. *Biochemistry* **2005**, *44*, 5525.

(39) Guillen, J.; Perez-Berna, A. J.; Moreno, M. R.; Villalain, J. *J. Virol.* **2005**, *79*, 1743.
(40) Sainz, B., Jr.; Rausch, J. M.; Gallaher, W. R.; Garry, R. F.; Wimley, W. C. *Biochemistry* **2005**, *44*, 947.
(41) Surewicz, W. K.; Mantsch, H. H.; Chapman, D. *Biochemistry* **1993**, *32*, 389.
(42) Zhang, Y. P.; Lewis, R. N.; Hodges, R. S.; McElhaney, R. N. *Biochemistry* **1992**, *31*, 11572.
(43) Muller, C.; Kukel, S.; Schneweis, K. E.; Bauer, R. *Clin. Exp. Immunol.* **1994**, *97*, 367.
(44) Bligh, E. G.; Dyer, W. J. *Can. J. Biochem. Physiol.* **1959**, *37*, 911.
(45) Mayer, L. D.; Bally, M. B.; Hope, M. J.; Cullis, P. R. *Chem. Phys. Lipids* **1986**, *40*, 333.
(46) Palestini, P.; Calvi, C.; Conforti, E.; Botto, L.; Fenoglio, C.; Miserocchi, G. *Am. J. Physiol.: Lung Cell Mol. Physiol.* **2002**, *282*, L1382.
(47) Böttcher, C. S. F.; Van Gent, C. M.; Fries, C. *Anal. Chim. Acta* **1961**, *1061*, 203.
(48) Edelhoch, H. *Biochemistry* **1967**, *6*, 1948.
(49) Bernabeu, A.; Guillen, J.; Perez-Berna, A. J.; Moreno, M. R.; Villalain, J. *Biochim. Biophys. Acta* **2007**, *1768*, 1659.
(50) Moreno, M. R.; Giudici, M.; Villalain, J. *Biochim. Biophys. Acta* **2006**, *1758*, 111.
(51) Meers, P.; Ali, S.; Erukulla, R.; Janoff, A. S. *Biochim. Biophys. Acta* **2000**, *1467*, 227.
(52) Sainz, B., Jr.; Rausch, J. M.; Gallaher, W. R.; Garry, R. F.; Wimley, W. C. *J. Virol.* **2005**, *79*, 7195.
(53) Eftink, M. R.; Ghiron, C. A. *Biochemistry* **1977**, *16*, 5546.
(54) Castanho, M.; Prieto, M. *Biophys. J.* **1995**, *69*, 155.
(55) Wardlaw, J. R.; Sawyer, W. H.; Ghiggino, K. P. *FEBS Lett.* **1987**, *223*, 20.
(56) Santos, N. C.; Prieto, M.; Castanho, M. A. *Biochemistry* **1998**, *37*, 8674.
(57) Contreras, L. M.; Aranda, F. J.; Gavilanes, F.; Gonzalez-Ros, J. M.; Villalain, J. *Biochemistry* **2001**, *40*, 3196.
(58) Pascual, R.; Moreno, M. R.; Villalain, J. *J. Virol.* **2005**, *79*, 5142.
(59) Giudici, M.; Pascual, R.; de la Canal, L.; Pfuller, K.; Pfuller, U.; Villalain, J. *Biophys. J.* **2003**, *85*, 971.
(60) Kauppinen, J. K.; Moffatt, D. J.; Mantsch, H. H.; Cameron, D. G. *Anal. Chem.* **1981**, *53*, 1454.
(61) Cameron, D. G.; Moffatt, D. J. *J. Test. Eval.* **1984**, *12*, 78.
(62) Pascual, R.; Contreras, M.; Fedorov, A.; Prieto, M.; Villalain, J. *Biochemistry* **2005**, *44*, 14275.
(63) Struck, D. K.; Hoekstra, D.; Pagano, R. E. *Biochemistry* **1981**, *20*, 4093.
(64) Lentz, B. R. *Chem. Phys. Lipids* **1993**, *64*, 99.
(65) Davenport, L.; Dale, R. E.; Bisby, R. H.; Cundall, R. B. *Biochemistry* **1985**, *24*, 4097.
(66) Pebay-Peyroula, E.; Dufourc, E. J.; Szabo, A. G. *Biophys. Chem.* **1994**, *53*, 45.
(67) Byler, D. M.; Susi, H. *Biopolymers* **1986**, *25*, 469.
(68) Arrondo, J. L.; Goni, F. M. *Prog. Biophys. Mol. Biol.* **1999**, *72*, 367.
(69) Roque, A.; Iloro, I.; Ponte, I.; Arrondo, J. L.; Suau, P. *J. Biol. Chem.* **2005**, *280*, 32141.
(70) Hofmann, H.; Pohlmann, S. *Trends Microbiol.* **2004**, *12*, 466.
(71) Sainz, B., Jr.; Mossel, E. C.; Gallaher, W. R.; Wimley, W. C.; Peters, C. J.; Wilson, R. B.; Garry, R. F. *Virus Res.* **2006**, *120*, 146.
(72) Zimmerberg, J.; Chernomordik, L. V. *Adv. Drug Delivery Rev.* **1999**, *38*, 197.
(73) Perez-Berna, A. J.; Moreno, M. R.; Guillen, J.; Bernabeu, A.; Villalain, J. *Biochemistry* **2006**, *45*, 3755.
(74) Lorizate, M.; de la Arada, I.; Huarte, N.; Sanchez-Martinez, S.; de la Torre, B. G.; Andreu, D.; Arrondo, J. L.; Nieva, J. L. *Biochemistry* **2006**, *45*, 14337.
(75) Gomara, M. J.; Mora, P.; Mingarro, I.; Nieva, J. L. *FEBS Lett.* **2004**, *569*, 261.
(76) Korazim, O.; Sackett, K.; Shai, Y. *J. Mol. Biol.* **2006**, *364*, 1103.
(77) Rabenstein, M.; Shin, Y. K. *Biochemistry* **1995**, *34*, 13390.
(78) Broer, R.; Boson, B.; Spaan, W.; Cosset, F. L.; Corver, J. *J. Virol.* **2006**, *80*, 1302.
(79) Chernomordik, L. V.; Kozlov, M. M. *Annu. Rev. Biochem.* **2003**, *72*, 175.